Journal of Clinical and Translational Hepatology **2026**
DOI: 10.14218/JCTH.2025.00658

Original Article

GSTM3 Knockdown Promotes Liver Fibrosis Reversal by Inhibiting Hepatic Stellate Cell Activation via PPARγ Signaling

Chenxue Hou[1#], Bingqing Yang[2#], Yuanying Zhao[1], Hao Chang[1], Tong Bu[2], Qi Wang[2*] and Yue Li[1*]

[1]Department of Clinical Laboratory, Beijing Ditan Hospital, Capital Medical University, Beijing, China; [2]Center of Liver Diseases, Beijing Ditan Hospital, Capital Medical University, Beijing, China

Received: December 03, 2025 | **Revised:** February 22, 2026 | **Accepted:** April 27, 2026 | **Published online:** May 25, 2026

Abstract

Background and Aims: Liver fibrosis is a pivotal and reversible stage in the progression of chronic liver disease. However, the mechanisms underlying fibrosis reversal remain unclear, and effective diagnostic biomarkers are lacking in clinical practice. In this study, we aimed to elucidate the role and molecular mechanisms of glutathione S-transferase Mu 3 (GSTM3) in liver fibrosis reversal, and preliminarily determine whether GSTM3 can serve as a novel biomarker for liver fibrosis reversal. ***Methods:*** Carbon tetrachloride-induced mouse models of liver fibrosis and spontaneous reversal were established. Proteomic analysis was used to identify proteins shared between liver tissue and serum that were continuously downregulated during fibrosis reversal. The expression of GSTM3 was evaluated in the livers of mice undergoing fibrosis reversal and in clinical samples from patients with liver fibrosis. Hepatic stellate cells (HSCs) were transfected with *Gstm3*-silencing RNA or an overexpression plasmid to assess the effects on fibrosis markers. RNA sequencing analyses were performed, and the underlying molecular mechanisms were investigated. ***Results:*** Proteomic analysis revealed significantly decreased GSTM3 levels in both hepatic tissue and serum in mice undergoing fibrosis reversal, and its expression was negatively correlated with the extent of reversal. GSTM3 levels were markedly increased in the hepatic tissue and serum of patients with liver fibrosis. GSTM3 expression was upregulated in transforming growth factor-β-stimulated HSCs. GSTM3 knockdown inhibited the expression of fibrosis markers, such as collagen type I α1 and tissue inhibitor of metalloproteinase 1, whereas its overexpression promoted their expression. Mechanistic studies indicated that GSTM3 knockdown activated peroxisome proliferator-activated receptor γ (PPARγ) signaling and downregulated its downstream targets, cluster of differentiation 36 and fatty acid-binding protein 4, thereby suppressing HSC activation. ***Conclusions:*** GSTM3 knockdown promotes liver fibrosis reversal via PPARγ signaling-mediated inhibition of HSC activation. Therefore, GSTM3 is a promising therapeutic target and diagnostic biomarker for liver fibrosis.

Citation of this article: Hou C, Yang B, Zhao Y, Chang H, Bu T, Wang Q, *et al*. GSTM3 Knockdown Promotes Liver Fibrosis Reversal by Inhibiting Hepatic Stellate Cell Activation via PPARγ Signaling. J Clin Transl Hepatol 2026. doi: 10.14218/JCTH.2025.00658.

Introduction

Liver fibrosis is a pathological result of dysregulated repair following chronic liver injury caused by various pathogenic factors, including viruses, metabolic disorders, and immune-mediated injury. It is an important link in the occurrence and development of chronic liver diseases and a common pathological process that progresses to liver cirrhosis, liver failure, and even hepatocellular carcinoma (HCC).[1–3] Worldwide, more than two million people die of liver disease each year, accounting for 4% of total deaths.[4,5] As the fourth leading cause of cancer-related deaths worldwide, HCC develops through a progression from hepatitis to liver fibrosis and cirrhosis in 80–90% of cases.[6] Clinical studies have shown that long-term antiviral therapy can reduce or even reverse liver fibrosis in patients infected with hepatitis B virus.[7,8] Furthermore, in recent years, several studies have confirmed that liver fibrosis is a dynamically reversible pathological process. When pathogenic factors are removed or effectively controlled, the progression of liver fibrosis can be delayed or even reversed.[9–11] However, the molecular mechanisms underlying liver fibrosis reversal remain unclear. In addition, effective molecular markers for dynamic monitoring are still lacking. Therefore, an in-depth exploration of the mechanisms underlying liver fibrosis reversal and the identification of molecular markers for dynamic monitoring and therapeutic targets are of great clinical significance for improving the prognosis of patients with liver fibrosis.

Glutathione S-transferase (GST) comprises a class of phase II metabolic enzymes that detoxify exogenous compounds. GST catalyzes the conjugation of glutathione with various electrophilic compounds and participates in the detoxification of carcinogens and the metabolism of various bioactive compounds.[12] The GST family is highly polymorphic, and allelic gene mutations or specific base deletions can increase susceptibility to cancer.[13,14] As a member of the GST family, glutathione S-transferase Mu 3 (GSTM3) plays an im-

Keywords: Glutathione S-transferase Mu 3; GSTM3; Liver fibrosis reversal; Hepatic stellate cells; HSCs; PPARγ signaling pathway.

[#]Contributed equally to this work.

[*]**Correspondence to:** Yue Li, Department of Clinical Laboratory, Beijing Ditan Hospital, Capital Medical University, Beijing 100015, China. ORCID: https://orcid.org/0000-0002-7412-7632. Tel: +86-10-84322438, E-mail: liyuedl04@126.com; Qi Wang, Center of Liver Diseases, Beijing Ditan Hospital, Capital Medical University, Beijing 100015, China. ORCID: https://orcid.org/0000-0002-0269-1568. Tel: +86-10-84322816, E-mail: wangqidl04@ccmu.edu.cn.

Table 1. Clinical characteristics of patients with different liver fibrosis stages

	Liver fibrosis S0 (n = 9)	Liver fibrosis S1–2 (n = 14)	Liver fibrosis S3–4 (n = 21)
Sex (F/M), n	5/4	7/7	14/7
Age, years	41.50 ± 16.35	49.18 ± 16.04	49.00 ± 15.03
ALT, U/L	24.25 (17.30,81.00)	67.50 (30.30,166.00)	38.80 (18.40, 84.35)
AST, U/L	19.20 (16.63,76.33)	50.80 (28.20,169.10)	49.70 (27.90,74.10)
GGT, U/L	18.55 (16.53,81.73)	40.70 (19.80,91.40)	51.10 (19.40,78.70)
ALP, U/L	89.30 (64.33,135.50)	66.50 (56.10,86.80)	73.50 (63.60,132.30)
ALB, g/L	44.70 (41.30, 46.50)	45.05 (40.08, 47.75)	40.20 (34.13, 44.20)
Liver histology			
Lobular inflammation (0/1/2/3/4), n	9/0/0/0/0	0/6/3/4/1	0/1/4/12/4
Fibrosis (0/1/2/3/4), n	9/0/0/0/0	0/4/10/0/0	0/0/0/7/14

This table presents the clinical characteristics and laboratory parameters of patients at different stages of liver fibrosis (S0, S1–2, S3–4). Data are presented as mean ± standard deviation or median (IQR). F, female; M, male; ALT, alanine aminotransferase; AST, aspartate aminotransferase; GGT, gamma-glutamyl transferase; ALP, alkaline phosphatase; ALB, albumin.

portant role in the detoxification of electrophilic compounds (e.g., toxins and carcinogens) and in the production of oxidative stress.[15,16] Several studies have shown that GSTM3 expression increases to varying degrees in various diseases. Meding *et al*. reported that high GSTM3 expression is associated with colorectal cancer occurrence, progression, and lymph node metastasis, whereas low GSTM3 expression is correlated with better survival.[17] However, in other diseases, GSTM3 expression is significantly decreased. Chen *et al*. found that low GSTM3 expression conferred a higher risk of local recurrence and predicted poor overall and progression-free survival in patients with nasopharyngeal carcinoma.[18] Zhang *et al*. evaluated the diagnostic ability of hub genes in three datasets using receiver operating characteristic (ROC) curves and found that GSTM3 was expressed at low levels in prostate cancer.[19] Guo *et al*. demonstrated that GSTM3 promoted liver cancer by inhibiting ferroptosis and that inhibiting GSTM3 activity reduced the incidence of liver cancer fourfold.[20] Through transcriptomic and proteomic analyses, Zhang *et al*. confirmed that the GSTM3 expression level in a mouse model of liver fibrosis was significantly higher than that in the normal group, suggesting that GSTM3 may be involved in the pathological process of liver fibrosis.[21] Although changes in GSTM3 expression are closely associated with the occurrence, development, and prognosis of various diseases, its specific roles and molecular mechanisms in liver fibrosis, particularly in its progression and reversal, remain unclear.

Peroxisome proliferator-activated receptor γ (PPARγ) is a key factor in maintaining the quiescent phenotype of hepatic stellate cells (HSCs). During liver fibrosis progression, both the expression and transcriptional activity of PPARγ in HSCs are markedly downregulated. In contrast, PPARγ activation can induce the transition to a quiescent phenotype and reduce the expression of fibrosis markers, such as α-smooth muscle actin (α-SMA) and collagen type I α1 (COL1A1). Therefore, PPARγ is considered an important regulatory node in anti-fibrotic responses.[22,23] Fatty acid-binding protein 4 (*FABP4*) and cluster of differentiation 36 (*CD36*) are canonical downstream target genes of PPARγ and play important roles in lipid metabolism, inflammatory responses, and oxidative stress.[24–26] However, the regulatory mechanisms of this signaling axis during the reversal phase of liver fibrosis remain insufficiently characterized, and the molecular association between this axis and GSTM3 remains unclear.

In this study, we systematically characterized the role of GSTM3 in liver fibrosis reversal using transcriptomic and proteomic analyses and ascertained whether it participates in the reversal of liver fibrosis by regulating the PPARγ-CD36-FABP4 axis. Notably, we investigated its effects on HSC activation, liver fibrosis reversal, and the underlying molecular mechanisms.

Methods

Patient samples

Liver and serum samples were collected from Beijing Ditan Hospital, Capital Medical University. Liver samples were obtained from 44 patients with biopsy-confirmed liver fibrosis. All patients were initially evaluated by clinicians, and the diagnosis was subsequently confirmed histopathologically. Liver biopsy sections were assessed independently in a blinded manner by two expert hepatopathologists, and fibrosis stage was determined according to the Scheuer scoring system (S0, no liver fibrosis; S1, portal fibrosis without septa; S2, portal fibrosis with a few septa; S3, numerous septa without architectural distortion or pseudolobule formation; and S4, extensive septa with pseudolobule formation consistent with cirrhosis).

Serum samples were obtained from 276 patients with liver fibrosis and 99 healthy controls who visited or were hospitalized at Beijing Ditan Hospital between October 2022 and September 2025. Baseline patient information is shown in Tables 1–3.

Animal models

For the spontaneous liver fibrosis reversal model, 8-week-old wild-type male mice (C57BL/6J; Beijing Saiye Biotechnology Co., Ltd.) were randomly divided into the control, carbon tetrachloride (CCl_4), reversal-4W, and reversal-12W groups. Mice in the CCl_4 and reversal groups were intraperitoneally injected with 12.5% CCl_4 solution (CCl_4:oil = 1:7, v/v) at 0.01 mL/g body weight twice weekly for 8 weeks to induce fibrosis, whereas the control group received an equal volume of oil injections.[27,28] Thereafter, CCl_4 administration was discontinued, and the reversal groups underwent spontaneous reversal for 4 and 12 weeks.

After treatment, the mice were euthanized, and serum and liver tissues were collected for analysis. All mice were

Table 2. Clinical characteristics of healthy controls and patients with different liver fibrosis stages

	Healthy control (n = 99)	Liver fibrosis S1–2 (n = 104)	Liver fibrosis S3–4 (n = 76)
Sex(F/M), n	91/8	61/43	37/39
Age, years	36.34 ± 9.07	45.66 ± 13.57	54.17 ± 10.55
ALT, U/L	14.00 (10.80,18.40)	42.10 (20.00,99.50)	39.15 (25.80,86.70)
AST, U/L	16.30 (13.75,18.75)	32.30 (21.50,62.80)	42.70 (29.70,79.48)
GGT, U/L	/	36.10 (19.85,77.55)	53.30 (31.60,102.30)
ALP, U/L	/	86.60 (74.60,134.60)	100.30 (83.43,131.90)
ALB, g/L	45.95 (44.40, 47.38)	44.80 (41.60, 47.60)	40.70 (35.38, 44.60)
Liver histology			
Lobular inflammation (0/1/2/3/4), n	/	0/59/41/4/0	0/6/32/34/4
Fibrosis (0/1/2/3/4), n	/	0/48/56/0/0	0/0/0/38/38

This table presents the clinical characteristics and laboratory parameters of HCs and patients at different stages of liver fibrosis (S1–2, S3–4). Data are presented as mean ± standard deviation or median (IQR). F, female; M, male; ALT, alanine aminotransferase; AST, aspartate aminotransferase; GGT, gamma-glutamyl transferase; ALP, alkaline phosphatase; ALB, albumin; HCs, healthy controls.

housed in a temperature-controlled environment under a 12-h light/12-h dark cycle and received food and water *ad libitum* at the Institute of Analysis and Testing, Beijing Academy of Science and Technology.

Cell culture and treatment

The human HSC line (LX-2), human umbilical vein endothelial cells (HUVECs), and the human hepatoma cell line (Huh-7) were obtained from the Cell Resource Center of the Beijing Institute of Basic Medical Sciences, Chinese Academy of Medical Sciences. The cells were cultured in high-glucose Dulbecco's modified Eagle's medium supplemented with 10% fetal bovine serum and 1% penicillin–streptomycin solution at 37 °C in 5% CO_2.[29]

For GSTM3 knockdown, LX-2 cells were transfected with small interfering RNA (siRNA) targeting *Gstm3* mRNA (si-GSTM3; GACAUCAUAGAGAACCAAGUATT, UACUUGGUUCUC UAUGAUGUCTT) or negative control siRNA (UUCUCCGAA CGUGUCACGUTT, ACGUGACACGUUCGGAGAATT) for 12 h and were then either treated with 10 ng/mL transforming growth factor-β (TGF-β) for 24 h or left untreated. For GSTM3 overexpression, LX-2 cells were transfected with pcDNA3.1-GSTM3 or control plasmid for 24 h.[30]

Proteomic analysis

Serum and liver samples were collected from the CCl_4, reversal-4W, and reversal-12W groups. Sample processing and mass spectrometry detection were performed by Biotech Pack Scientific (Shanghai, China). Mass spectrometry analysis was conducted using a Thermo Astral instrument in data-independent acquisition mode with the following parameters: MS1, 380–980 m/z at 240 k resolution; and MS2, 150–2,000 m/z with 25% normalized collision energy and a 2 m/z isolation window.[31]

Histology

Paraffin sections of fixed tissues were stained with hematoxylin and eosin (H&E) and Masson's trichrome.[32] Detailed immunohistochemistry and immunofluorescence procedures have been described previously.[33] The antibodies used are listed in Supplementary Table 1.

Enzyme-linked immunosorbent assay (ELISA)

GSTM3 levels in human serum samples were measured using ELISA kits (orb778927; Biorbyt, UK).

Measurement of reactive oxygen species (ROS)

LX-2 cells were seeded into 6-well plates at a density of 2 × 10^4 cells per well and cultured for 24 h. Subsequently, 20 μM 2′,7′-dichlorofluorescein diacetate was added, and the cells were incubated at 37 °C for 30 min. Fluorescence intensity was observed and photographed under a microscope.[34]

Table 3. Clinical characteristics of healthy controls and patients with liver fibrosis or cirrhosis

	Healthy control (n = 99)	Liver fibrosis (n = 40)	Liver cirrhosis (n = 56)
Sex(F/M), n	91/8	23/17	11/45
Age, years	36.34 ± 9.07	41.48 ± 14.12	50.96 ± 12.37
ALT, U/L	14.00 (10.80,18.40)	80.70 (40.00,190.30)	24.30 (14.40,56.10)
AST, U/L	16.30 (13.75,18.75)	58.10 (31.28, 136.30)	32.90 (22.00, 66.20)
GGT, U/L	/	31.21 (18.05,83.05)	44.20 (23.20,130.20)
ALP, U/L	/	94.80 (79.78, 131.9)	112.80 (82.20, 133.40)
ALB, g/L	45.95 (44.40,47.38)	43.85 (39.55,47.28)	37.00 (31.80, 42.50)

This table presents the clinical characteristics and laboratory parameters of healthy controls HCs and patients at different stages of liver disease. Data are presented as mean ± standard deviation or median (IQR). F, female; M, male; ALT, alanine aminotransferase; AST, aspartate aminotransferase; GGT, gamma-glutamyl transferase; ALP, alkaline phosphatase; ALB, albumin; HCs, healthy controls.

Reverse transcription-quantitative polymerase chain reaction (RT-qPCR)

Total RNA was extracted using an RNA extraction kit (Dakewe Biotech, Shenzhen, China) and reverse-transcribed into cDNA using a PrimeScript™ RT reagent kit (TaKaRa, Shiga, Japan). qPCR was performed using Fast SYBR Green PCR Master Mix (Applied Biosystems, Waltham, MA, USA). Relative mRNA abundance was normalized to *Gapdh* expression.[35] The primer sequences are listed in Supplementary Table 2.

Western blotting

Western blotting was performed according to the standard sodium dodecyl sulfate–polyacrylamide gel electrophoresis protocol, followed by incubation with antibodies (Supplementary Table 1).[36]

RNA sequencing (RNA-seq)

LX-2 cells were transfected with si-GSTM3 and then treated with TGF-β. RNA-seq was performed by Shanghai Biotechnology Corporation using the Illumina NovaSeq 6000 platform. Differential expression analysis was conducted using edgeR, with a false discovery rate < 0.05 and |log2 fold change| > 1 as the thresholds for defining differentially expressed genes (DEGs), which were subjected to Gene Ontology (GO) annotation and Kyoto Encyclopedia of Genes and Genomes (KEGG) pathway enrichment analysis.[37]

Statistical analysis

Quantitative data with a normal distribution are presented as the mean ± standard deviation, whereas data with a non-normal distribution are expressed as the median (IQR) [M (P25, P75)]. Categorical variables are described as frequencies and percentages (n, %). For continuous quantitative data with a normal distribution and homogeneous variances, between-group comparisons were performed using Student's *t*-test, and multiple-group comparisons were conducted using one-way analysis of variance. For non-normally distributed data, the Mann–Whitney *U* test or Kruskal–Wallis test was applied as appropriate. Data processing and statistical graphing were performed using GraphPad Prism (version 9.5; GraphPad Software, San Diego, CA, USA). Statistical significance was defined as a two-tailed *P*-value < 0.05.

Ethical approval

All protocols and animal studies were conducted in accordance with the Guide for the Care and Use of Laboratory Animals of the US National Institutes of Health (NIH Publication No. 85-23; National Academies Press, 2011) and were approved by the Animal Experiments and Experimental Animal Welfare Committee of Capital Medical University (No. AEEI-2024-486). All animals received human care. The human study conformed to the ethical guidelines of the 2024 Declaration of Helsinki, as reflected in a priori approval by the Ethics Committee of Beijing Ditan Hospital (No. KY2021-046-03 and No. KY2025-015-03), and the Informed Consent Form for Medical Data and Biological Sample Donation. All participants provided written informed consent. All biological samples and clinical data included in this retrospective analysis were fully anonymized before use. No additional interventions that might compromise patients' rights, interests or welfare were performed. Furthermore, no biological materials were obtained from prisoners or other vulnerable institutionalized populations.

Results

Proteomic analysis identified differentially expressed proteins (DEPs) during mouse liver fibrosis reversal

To explore the molecular mechanisms underlying liver fibrosis reversal, we established a mouse model of CCl_4-induced liver fibrosis, followed by spontaneous reversal for 4 and 12 weeks. Histological analysis showed that the fibrosis reversal groups exhibited significant improvements in CCl_4-induced liver injury, including severe steatosis, inflammatory cell infiltration, and collagen deposition (Fig. 1A). Consistent with the histological changes, the expression levels of the key fibrosis markers α-SMA and COL1A1 were significantly elevated in fibrotic livers but decreased in a time-dependent manner during spontaneous reversal. The levels in the reversal-12W group were similar to those in the control group, as evidenced by immunohistochemistry, immunofluorescence, and western blotting (Fig. 1A–D). These findings indicate that, concomitant with fibrosis reversal, the number of activated HSCs decreased and their activity was suppressed. Collectively, these morphological and molecular data demonstrate that we successfully established a mouse model of liver fibrosis with robust spontaneous reversal.

Next, we performed proteomic analyses of liver tissue and serum samples collected from mice in the CCl_4, reversal-4W, and reversal-12W groups. Dynamic comparisons of protein expression profiles across these three groups identified 1,236 DEPs in the serum and 2,037 DEPs in the liver tissue (Fig. 1E). KEGG pathway enrichment analysis of the DEPs revealed distinct functional patterns between serum and liver tissue during liver fibrosis reversal. In serum, DEPs were mainly enriched in pathways related to proteasomes, ribosomes, phagosomes, and endocytosis, suggesting that the regulation of protein metabolism and immune responses at the systemic level contributed to the regression of fibrosis (Fig. 1F). Consistently, GO annotation showed that serum DEPs were primarily involved in biological processes such as organic nitrogen compound metabolism, macromolecule localization, and protein degradation, whereas their molecular functions were largely associated with protein binding, catalytic activity, and small-molecule binding (Fig. 1G). In contrast, DEPs in the liver tissue were significantly enriched in metabolism-related pathways, including central metabolic pathways, pyruvate metabolism, fatty acid metabolism, and branched-chain amino acid metabolism (Fig. 1H). GO analysis further indicated that biological processes in the liver were predominantly related to diverse metabolic activities, including organic substance metabolism, cellular metabolism, and small-molecule metabolic processes, which were mainly enriched in catalytic activity, ion binding, and protein binding (Fig. 1I). These findings suggest that peripheral circulation and local hepatic tissue contribute to liver fibrosis reversal through distinct molecular mechanisms. Serum primarily reflects systemic alterations in protein metabolism and immune regulation, whereas the liver undergoes metabolic network reprogramming.

GSTM3 was a continuously downregulated DEP in both liver tissue and serum during mouse liver fibrosis reversal

To identify key molecules involved in liver fibrosis reversal, we performed KEGG pathway enrichment and GO annotation analyses on 424 commonly expressed proteins in both liver tissue and serum. These proteins were primarily enriched in critical metabolic pathways, including carbon, glutathione, amino acid, and nucleotide sugar metabolism, suggesting

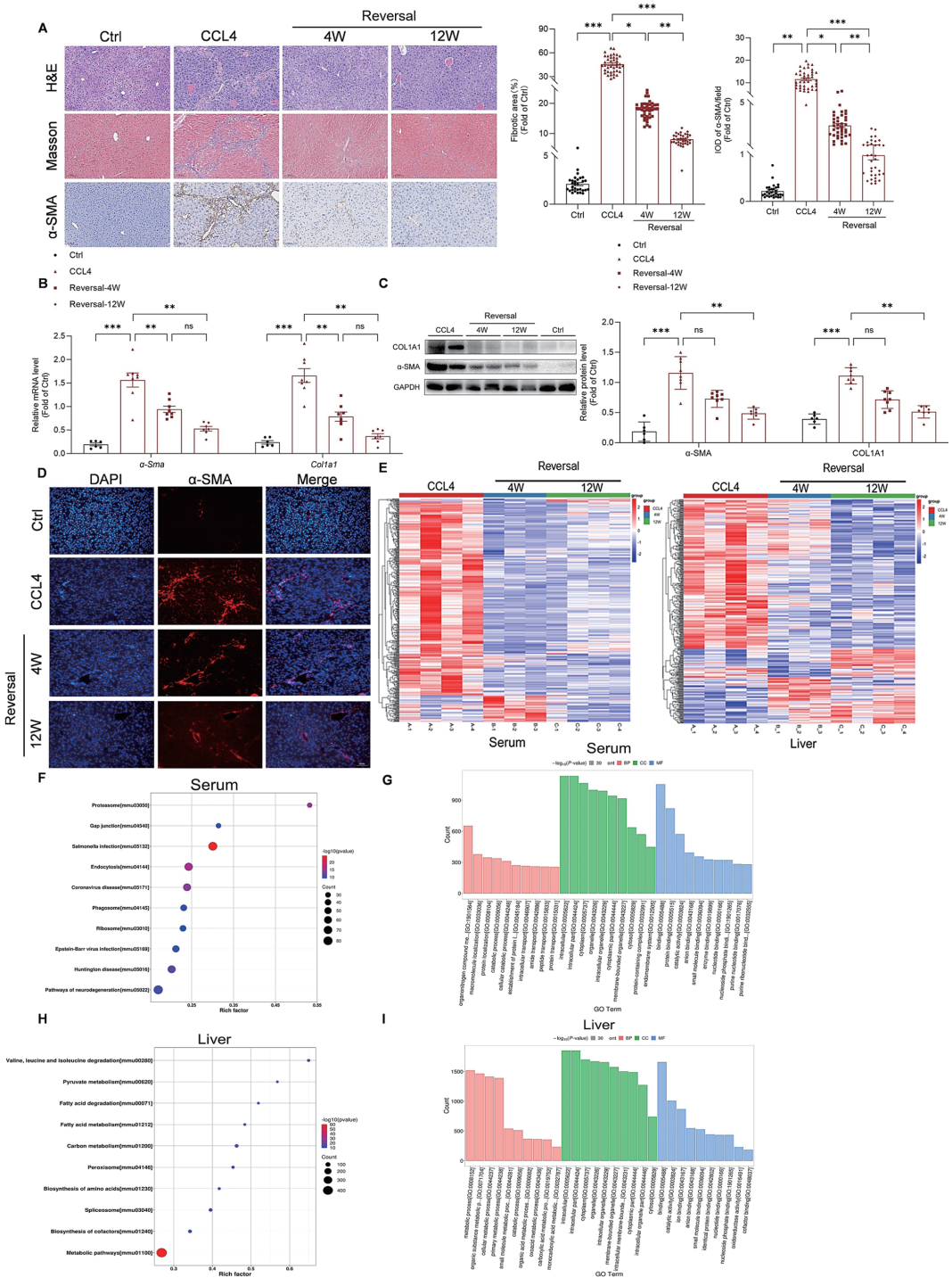

Fig. 1. Proteomic profiling of liver and serum in a mouse model of liver fibrosis reversal. (A–D) Wild-type mice (Ctrl) were subjected to CCl_4-induced liver fibrosis, followed by a spontaneous recovery period of 4 weeks (reversal-4W) or 12 weeks (reversal-12W). (A) Representative images of H&E and Masson's trichrome staining and immunohistochemistry for α-SMA in liver tissues from the Ctrl (n = 6), CCl_4 (n = 8), reversal-4W (n = 8), and reversal-12W (n = 7) groups. (B) RT-qPCR analysis of the mRNA levels of *α-Sma* and *Col1a1* in the liver. (C) Western blot analysis of COL1A1 and α-SMA protein levels in the liver. (D) Representative immunofluorescence staining for α-SMA in liver tissues. (E) Heatmap of DEPs in the serum and liver tissues of mice in the CCl_4 (n = 4), reversal-4W (n = 3), and reversal-12W (n = 4) groups. (F) KEGG enrichment analysis of serum DEPs and the top 10 significantly enriched pathways based on *P*-values. (G) GO functional annotation analysis of DEPs in serum. (H) KEGG enrichment analysis of liver DEPs and the top 10 significantly enriched pathways based on *P*-values. (I) GO functional annotation analysis of DEPs in liver tissue. Data are presented as mean ± standard error of the mean (SEM) (*P < 0.05; **P < 0.01; ***P < 0.001; ns, not significant). *P*-values were obtained using an unpaired *t*-test. Ctrl, control; CCl_4, carbon tetrachloride; H&E, hematoxylin and eosin; α-SMA, α-smooth muscle actin; RT-qPCR, reverse transcription quantitative polymerase chain reaction; COL1A1, collagen type I alpha 1 chain; DEPs, differentially expressed proteins; KEGG, Kyoto Encyclopedia of Genes and Genomes; GO, Gene Ontology; SEM, standard error of the mean; ns, not significant.

that metabolic reprogramming plays a central role in liver fibrosis reversal (Fig. 2A). GO annotation further indicated that these commonly downregulated proteins were mainly involved in biological processes such as cellular metabolism, organic substance metabolism, and small-molecule metabolic processes, with molecular functions predominantly related to catalytic and binding activities (Fig. 2B).

Accordingly, we constructed a protein–protein interaction (PPI) network of the shared DEPs in liver tissue and serum during liver fibrosis reversal (Fig. 2C). Cross-comparison identified several shared proteins, including GSTM3, ALOX15, and RIPK3, whose expression decreased during reversal in both compartments. Western blot validation and expression pattern analyses revealed that GSTM3 was the only protein that exhibited continuous, stepwise downregulation in both liver tissue and serum. Heatmap visualization further revealed that GSTM3 expression was highest in the liver tissue and serum of the CCl_4 group and showed a pronounced stepwise decline during spontaneous reversal (Fig. 2D and E). Collectively, these results suggest that GSTM3 is not only involved in the development and progression of liver fibrosis but may also represent a key functional regulator of the reversal process.

GSTM3 was highly expressed in fibrotic mouse liver but gradually decreased in the fibrosis reversal model

To validate the proteomic findings, we systematically assessed GSTM3 protein expression in liver tissue using immunohistochemistry and western blotting. GSTM3 protein expression was upregulated in the CCl_4 group but decreased in a time-dependent manner during spontaneous fibrosis reversal. In particular, GSTM3 expression approached baseline levels in the reversal-12W group (Fig. 3A–C). These data indicate a significant negative association between GSTM3 expression and the extent of liver fibrosis reversal.

Immunohistochemical staining revealed that GSTM3 was mainly upregulated in non-parenchymal cells of the fibrotic liver (Fig. 3A). Western blot analysis showed that GSTM3 was predominantly expressed in LX-2 cells, moderately expressed in HUVECs, and barely detectable in Huh-7 cells (Fig. 3D). Immunofluorescence was performed to determine the subcellular localization of GSTM3 in LX-2 cells. The results showed that GSTM3 was primarily localized to the cytoplasm (Fig. 3E). These findings suggest that GSTM3 expression may play a role in both the progression and reversal of fibrosis in patients with liver fibrosis. This provides important insights for the subsequent investigation of the downstream molecular mechanisms regulated by GSTM3.

GSTM3 was increased in the serum and liver tissues of patients with fibrosis

To explore the role of GSTM3 in liver fibrosis, liver biopsy specimens were collected from 44 patients with liver fibrosis, and GSTM3 expression was evaluated using immunohistochemical staining. According to the modified Scheuer scoring system, the samples were classified into S0, S1–2, and S3–4 groups. Liver samples from patients with fibrosis showed increased collagen deposition and inflammatory cell infiltration, as indicated by H&E and Masson's trichrome staining. We found that GSTM3 levels were higher in patients with fibrosis than in those in the S0 group. In particular, GSTM3 expression was associated with fibrosis stage, and patients with S3–4 fibrosis showed higher GSTM3 expression than those in the other groups (Fig. 4A). This stepwise increase suggests that GSTM3 is involved in the progression of liver fibrosis and is closely linked to disease severity.

To further demonstrate the effects of GSTM3 on fibrosis, we collected serum samples from 180 patients at different stages of liver fibrosis and from 99 healthy controls. GSTM3 levels were quantified in all serum samples using ELISA. Serum GSTM3 levels were 5.92 ng/mL in healthy controls and increased to 9.80 and 26.63 ng/mL in the S1–2 and S3–4 groups, respectively, indicating a clear stage-dependent elevation (Fig. 4B). This progressive upward trend was consistently validated across analyses using different grouping strategies (Fig. 4C–F). Notably, ROC curve analysis revealed that GSTM3 exhibited good diagnostic performance for significant liver fibrosis ($S \geq 2$), with an area under the ROC curve (AUC) of 0.8213 (Fig. 4G). Correlation analysis further demonstrated a significant positive association between GSTM3 levels and the widely used noninvasive Fibrosis-4 Index (FIB-4; $R = 0.8077$, $P < 0.01$; Fig. 4H), suggesting a high degree of concordance between GSTM3 and established clinical noninvasive assessments and further supporting its translational potential as a diagnostic biomarker.

To further validate GSTM3 expression across different severity levels of chronic liver disease, we expanded the clinical sample size by enrolling 96 patients with chronic liver disease (including those with liver fibrosis and cirrhosis). ELISA measurements showed that GSTM3 levels increased stepwise with disease severity; they increased to 18.69 ng/mL in the liver fibrosis group and reached 21.61 ng/mL in the cirrhosis group (Fig. 4I). ROC curve analysis indicated that GSTM3 achieved the best diagnostic performance in compensated cirrhosis, with an AUC of 0.8321, reflecting optimal diagnostic accuracy at this stage (Fig. 4J and K). This gradient pattern further indicates that GSTM3 is closely associated with liver fibrosis progression and remains highly expressed in patients with cirrhosis.

GSTM3 knockdown suppressed HSC activation and reduced ROS levels

HSC activation plays a critical role in the progression and regression of liver fibrosis.[1] Therefore, we investigated the effects of GSTM3 knockdown on HSC function. We knocked down GSTM3 in LX-2 cells using siRNA, which significantly reduced GSTM3 expression (Fig. 5A and B). GSTM3 knockdown significantly decreased the expression of fibrosis markers, including COL1A1, fibronectin, and tissue inhibitor of metalloproteinase 1 (TIMP1), suggesting that GSTM3 plays an important role in maintaining the activated phenotype of HSCs (Fig. 5C). These data indicate that GSTM3 deficiency may ameliorate liver fibrosis.

To investigate the regulatory role of GSTM3 downregulation in HSCs, we treated GSTM3-downregulated LX-2 cells with TGF-β to induce hepatic fibrosis *in vitro*. TGF-β treatment increased the mRNA levels of *α-Sma*, *Col1a1*, and *Timp1* in LX-2 cells, and these elevations were attenuated by GSTM3 knockdown (Fig. 5D). Consistent with this result, the protein levels of COL1A1, TIMP1, fibronectin, and elastin were lower in GSTM3-knockdown cells than in TGF-β-treated control cells (Fig. 5E). Immunofluorescence staining further confirmed that GSTM3 knockdown markedly reduced the fluorescence intensities of α-SMA and COL1A1, suggesting attenuation of LX-2 cell activation (Fig. 5F and G).

To determine whether GSTM3 regulates oxidative stress, we assessed intracellular ROS levels in LX-2 cells. Quantification of fluorescence intensity revealed that TGF-β stimulation markedly increased intracellular ROS levels compared with those in the control group. Notably, this TGF-β-induced ROS elevation was significantly attenuated by GSTM3 knockdown (Fig. 5H). These data confirm that GSTM3 knockdown suppressed oxidative stress in activated LX-2 cells, which may have contributed to the inhibition of hepatic fibrogenesis.

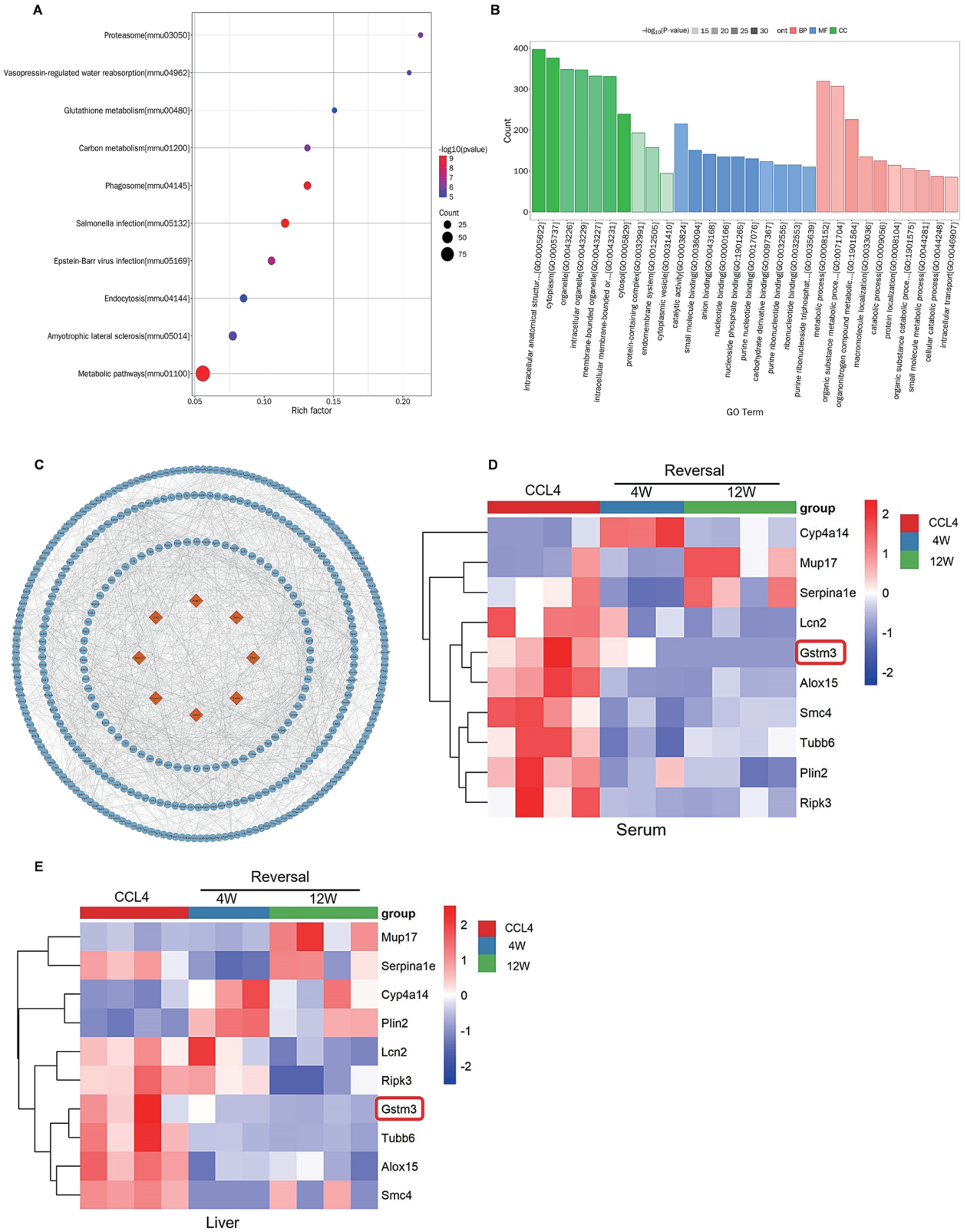

Fig. 2. Integrated bioinformatics analysis of DEPs shared between liver tissue and serum. (A) Top 10 KEGG pathways enriched in shared DEPs, ranked by *P*-value. (B) GO functional annotation analysis of shared DEPs. (C) PPI network of shared DEPs. (D, E) Heatmap of shared DEPs in serum (D) and liver tissue (E). DEPs, differentially expressed proteins; KEGG, Kyoto Encyclopedia of Genes and Genomes; GO, Gene Ontology; PPI, protein–protein interaction.

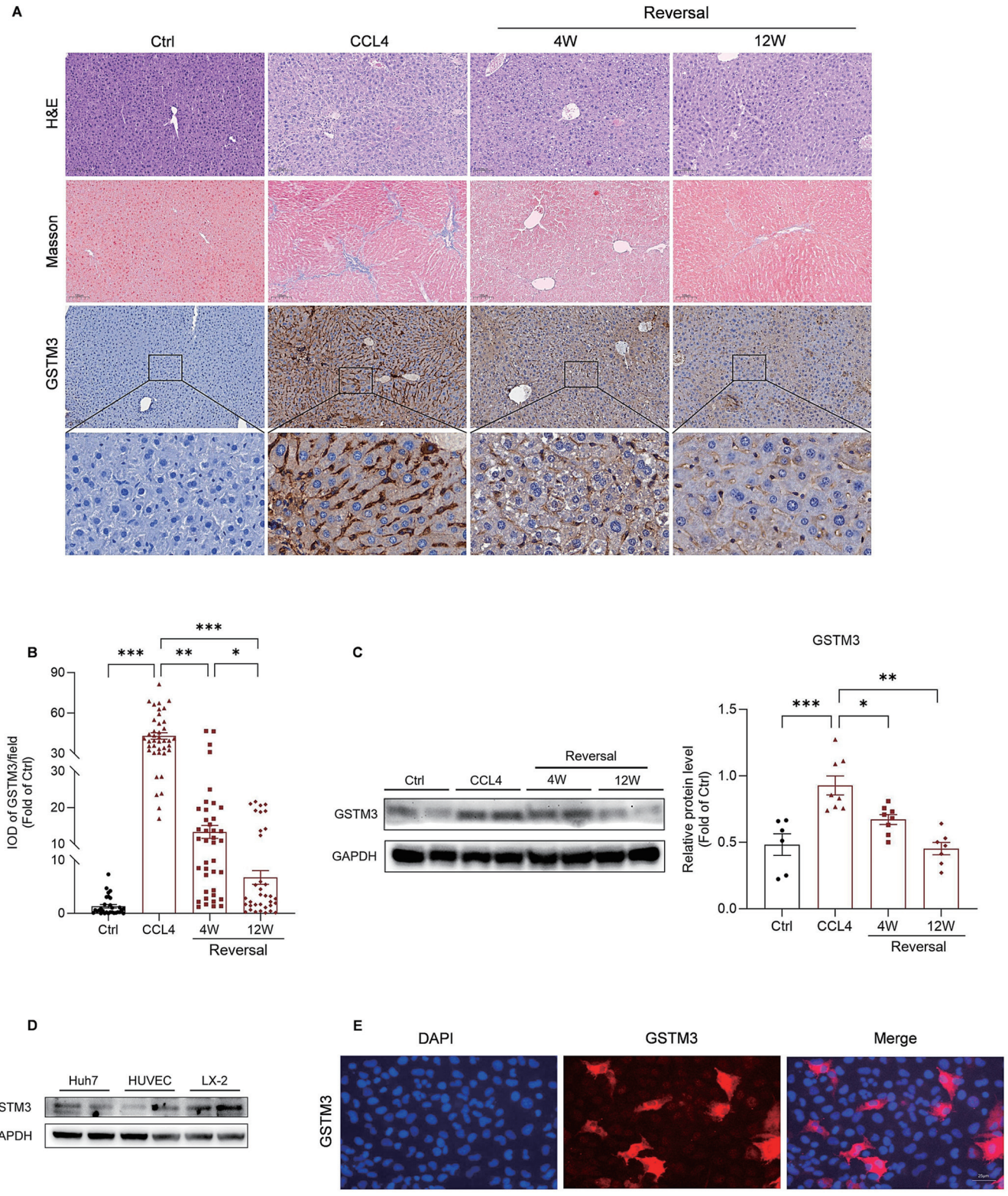

Fig. 3. Protein levels and localization of GSTM3 in mouse liver tissues and LX-2 cells. (A, B) Immunohistochemical GSTM3 staining in liver tissues of mouse models (n = 6–8 per group). (C) Western blot analysis of GSTM3 protein levels in liver tissues. (D) Western blot analysis of GSTM3 protein levels in cell lines. (E) Immunofluorescence staining of GSTM3 in LX-2 cells. Data are presented as mean ± SEM (*P < 0.05; **P < 0.01; ***P < 0.001). P-values were obtained using an unpaired t-test. GSTM3, glutathione S-transferase Mu 3; SEM, standard error of the mean; IOD, integrated optical density; GAPDH, glyceraldehyde-3-phosphate dehydrogenase.

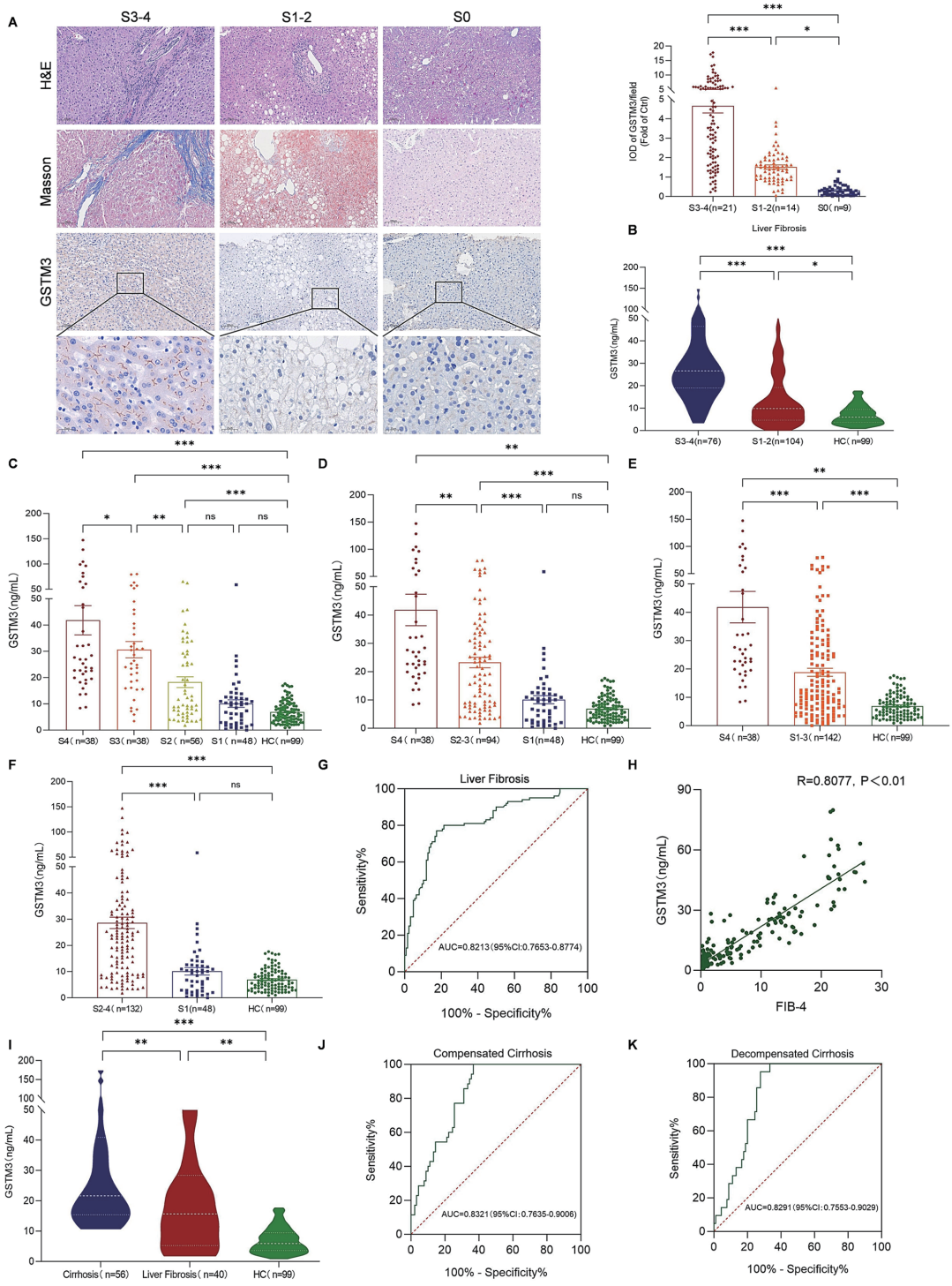

Fig. 4. Analysis of GSTM3 levels in the serum and liver tissues of patients with fibrosis. (A) H&E and Masson's trichrome staining and representative immunohistochemical staining of GSTM3 in liver sections of patients with fibrosis (n = 44) at different stages of fibrosis (S0: n = 9; S1–2: n = 14; S3–4: n = 21). (B) ELISA analysis of serum GSTM3 levels in HC (n = 99) and patients with fibrosis (n = 180) at different stages of fibrosis (S1–2: n = 104; S3–4: n = 76). (C–F) Stratified analyses of serum GSTM3 levels in patients with liver fibrosis at different stages. (G) ROC curve analysis of serum GSTM3 for identifying significant liver fibrosis (S ≥ 2). (H) Correlation analysis of serum GSTM3 levels and the fibrosis index, FIB-4. (I) ELISA analysis of serum GSTM3 levels in HC (n = 99), patients with liver fibrosis (n = 40), and patients with liver cirrhosis (n = 56). (J, K) ROC curve analyses of serum GSTM3 levels in patients with chronic liver disease at different disease stages. Comparisons between two groups were performed using the Mann–Whitney *U* test, and comparisons among multiple groups were performed using the Kruskal–Wallis *H* test. Correlation analysis was conducted using Spearman's rank correlation. Data are presented as mean ± SEM (ns, not significant; **P* < 0.05; ***P* < 0.01; ****P* < 0.001). *P*-values were obtained using an unpaired *t*-test. GSTM3, glutathione S-transferase Mu 3; H&E, hematoxylin and eosin; ELISA, enzyme-linked immunosorbent assay; HC, healthy controls; ROC, receiver operating characteristic; FIB-4, Fibrosis-4; SEM, standard error of the mean; ns, not significant.

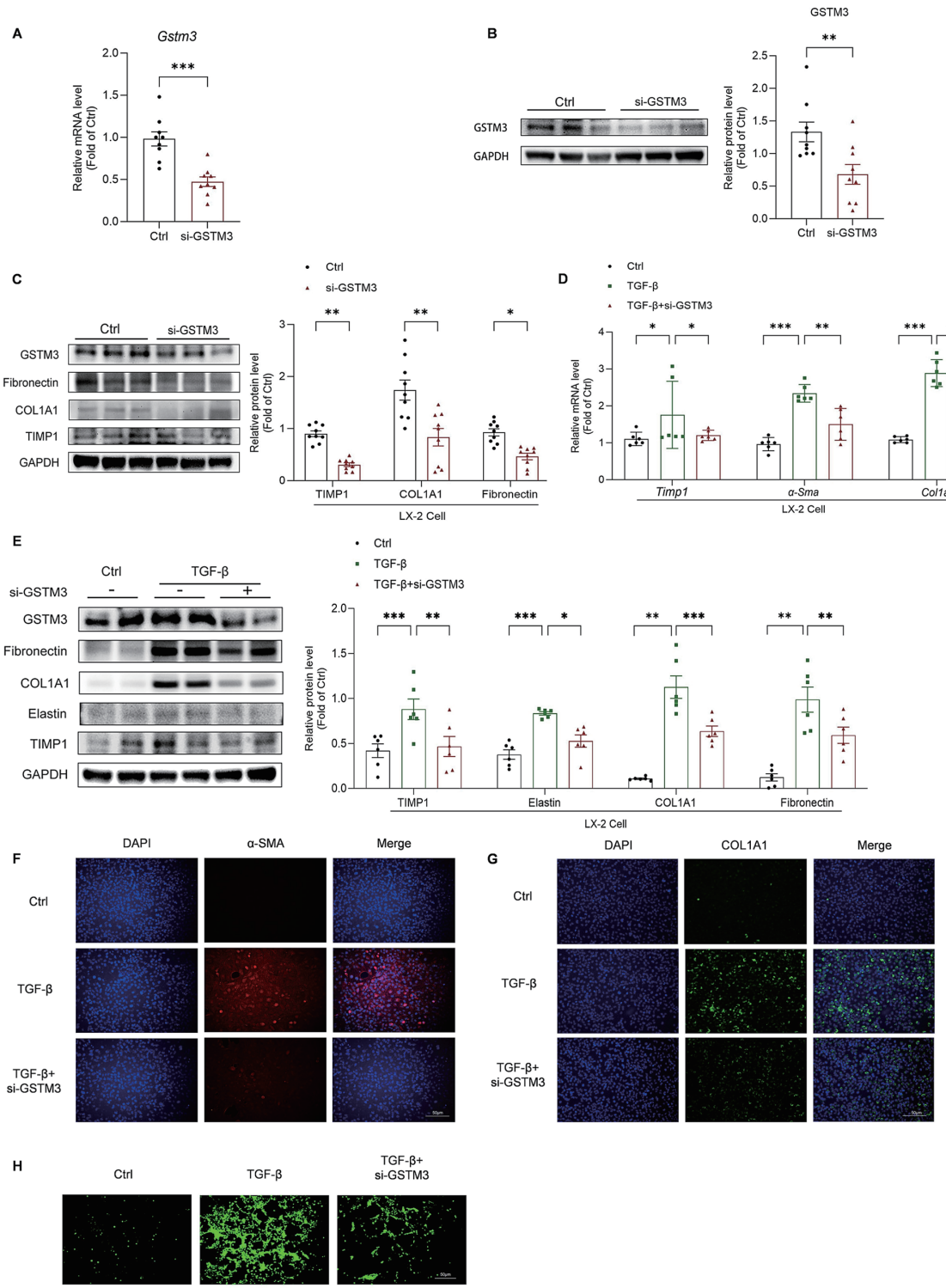

Fig. 5. Effects of GSTM3 knockdown on HSC activation and ROS levels in LX-2 cells. (A–C) LX-2 cells were transfected with si-GSTM3 for 24 h (n = 3). (A) RT-qPCR analysis of *Gstm3* mRNA expression levels. (B) Western blot analysis of GSTM3 protein levels. (C) Western blot analysis of TIMP1, COL1A1, and fibronectin levels. (D–H) LX-2 cells were transfected with si-GSTM3 for 12 h and then treated with or without TGF-β for 24 h (n = 3). (D) RT-qPCR analysis of *Timp1*, *Col1a1*, and *α-Sma* mRNA expression levels. (E) Western blot analysis of TIMP1, elastin, COL1A1, and fibronectin levels. (F, G) Immunofluorescence staining for α-SMA and COL1A1. (H) ROS levels in LX-2 cells. Data are presented as mean ± SEM (*P < 0.05; **P < 0.01; ***P < 0.001). P-values were obtained using an unpaired t-test. GSTM3, glutathione S-transferase Mu 3; HSC, hepatic stellate cell; ROS, reactive oxygen species; RT-qPCR, reverse transcription quantitative polymerase chain reaction; TIMP1, tissue inhibitor of metalloproteinases 1; COL1A1, collagen type I alpha 1 chain; TGF-β, transforming growth factor-β; α-SMA, α-smooth muscle actin; SEM, standard error of the mean; GAPDH, glyceraldehyde-3-phosphate dehydrogenase.

Taken together, these data indicate that GSTM3 knockdown suppresses HSC activation and ROS production.

Elevated GSTM3 promoted HSC activation and increased ROS levels

As shown in the liver sections from patients and mice with fibrosis, GSTM3 expression was upregulated (Figs. 3A and 4A). Next, we investigated the effects of GSTM3 overexpression on HSC activation. The pcDNA3.1-GSTM3 plasmid, which significantly increased GSTM3 expression, was constructed and transfected into LX-2 cells (Fig. 6A). GSTM3 overexpression increased the protein levels of fibrosis markers, including TIMP1, COL1A1, and α-SMA (Fig. 6B). Furthermore, the mRNA level of *Timp1* was upregulated in GSTM3-overexpressing cells (Fig. 6C). Immunofluorescence staining further demonstrated that GSTM3 overexpression markedly enhanced the fluorescence intensities of α-SMA and COL1A1, indicating that LX-2 cells were activated and exhibited an increased capacity for extracellular matrix synthesis (Fig. 6D and E).

Additionally, intracellular ROS measurements showed that ROS levels were significantly elevated in the GSTM3-overexpressing group (Fig. 6F). These results indicate that elevated GSTM3 levels promote HSC activation and increase ROS production.

GSTM3 knockdown suppressed HSC activation via the PPARγ signaling pathway

We investigated the mechanisms by which GSTM3 contributes to liver fibrosis and its reversal. LX-2 cells were treated with TGF-β in the presence or absence of si-GSTM3, followed by RNA-seq analysis. A total of 647 DEGs were identified following GSTM3 knockdown, including 318 upregulated and 329 downregulated genes. The expression profiles of these DEGs are shown in a heatmap and volcano plot (Fig. 7A and B). KEGG pathway enrichment analysis revealed that the DEGs were significantly enriched in pathways related to fibrosis, such as PPAR signaling, Ras signaling, and cancer pathways (Fig. 7C). GO functional annotation further indicated that these genes were primarily involved in key biological processes such as cellular processes, signal transduction, and biological regulation (Fig. 7D). Collectively, these results suggest that GSTM3 may regulate HSC activation by modulating pathways governing cellular architecture and signal transduction. Notably, systematic screening of the KEGG enrichment results, along with the findings of previous studies, highlighted the PPARγ signaling pathway as a key potential downstream mediator. Western blotting confirmed that GSTM3 knockdown markedly increased PPARγ expression.

PPARγ activation suppresses HSC activation and negatively regulates CD36 and FABP4.[38–41] We found that TGF-β treatment increased the protein levels of CD36 and FABP4 in LX-2 cells, and these elevations were attenuated by GSTM3 knockdown (Fig. 7E). These findings indicate that the inhibitory effect of GSTM3 knockdown on HSC activation is mediated, at least in part, by modulation of the PPARγ signaling pathway and its downstream targets, CD36 and FABP4.

Discussion

Liver fibrosis is a common pathological process in various chronic liver diseases that can progress to liver cirrhosis, liver failure, and HCC, conferring a heavy global health burden.[1–3] Although extensive studies have investigated the mechanisms underlying the progression of liver fibrosis, the molecular regulation of its spontaneous reversal remains unclear.[9–11] Currently, effective clinical therapies targeting the reversal of liver fibrosis are unavailable, and the key molecules and signaling pathways driving this reversible process remain unelucidated.[42–44]

To address these knowledge gaps and explore the molecular alterations and key regulators governing liver fibrosis reversal, we performed quantitative proteomic analyses of liver tissue and serum from CCl_4, reversal-4W, and reversal-12W mouse groups and identified 1,236 and 2,037 DEPs in the serum and liver tissue, respectively, with distinct expression patterns. KEGG and GO analyses revealed divergent functions: serum DEPs were enriched in proteasome, ribosome, phagosome, and endocytosis pathways, whereas liver DEPs were enriched in metabolic pathways (pyruvate, fatty acid, and branched-chain amino acid metabolism), indicating distinct molecular programs in the peripheral circulation and local liver tissue during reversal. Cross-comparison of the 424 shared DEPs and their PPI network identified several proteins—including GSTM3, ALOX15, and RIPK3—that were continuously downregulated during fibrosis reversal in both liver tissue and serum. Western blot analyses further confirmed that GSTM3 was the only protein that exhibited consistent stepwise downregulation in both compartments during the course of reversal, identifying it as a key candidate regulator of fibrosis reversal.

GSTM3, a member of the GST superfamily, is a critical detoxification enzyme that participates in cellular antioxidant defense and xenobiotic metabolism by scavenging ROS and conjugating toxic substances.[14–16] Accumulating evidence from previous studies has implicated GSTM3 in the pathogenesis of multiple human diseases, including various malignant tumors (e.g., HCC and colorectal cancer) and chronic inflammatory disorders.[17–20,45,46] However, the specific biological functions of GSTM3 in liver fibrosis, particularly in spontaneous fibrosis reversal, remain unknown. We found that GSTM3 expression gradually decreased during liver fibrosis reversal and was negatively correlated with fibrotic resolution in mouse models. Consistently, GSTM3 expression was elevated in the liver tissue and serum of patients with liver fibrosis, and its levels were positively correlated with fibrosis stage, in agreement with the expression pattern observed in mice.

As HSC activation and inactivation are critical events that determine the progression and reversal of liver fibrosis,[42,47–49] we further investigated the functional role of GSTM3 in LX-2 cells. Our *in vitro* experiments showed that GSTM3 knockdown reduced the expression of fibrosis markers (COL1A1, fibronectin, and TIMP1), attenuated TGF-β-induced HSC activation and extracellular matrix production, and suppressed intracellular ROS accumulation. In contrast, GSTM3 overexpression increased the expression of fibrotic genes, extracellular matrix synthesis, and ROS levels, thereby promoting a profibrotic phenotype. These results demonstrate that GSTM3 promotes HSC activation, whereas its downregulation suppresses HSC activation and facilitates the reversal of liver fibrosis. Therefore, GSTM3 may represent a potential therapeutic target for liver fibrosis. Although our *in vitro* experiments demonstrated that GSTM3 regulates HSC activation and oxidative stress, which may indirectly contribute to the reversal of liver fibrosis, these findings warrant validation *in vivo*.

Further studies using GSTM3-knockout mice in a liver fibrosis reversal model are warranted to directly confirm the role of GSTM3 in fibrosis resolution and clarify its precise mechanisms during the reversal process, thereby enhancing the reliability of these findings.

Next, we investigated the regulatory mechanisms of GSTM3 in fibrosis reversal. We performed RNA-seq on TGF-

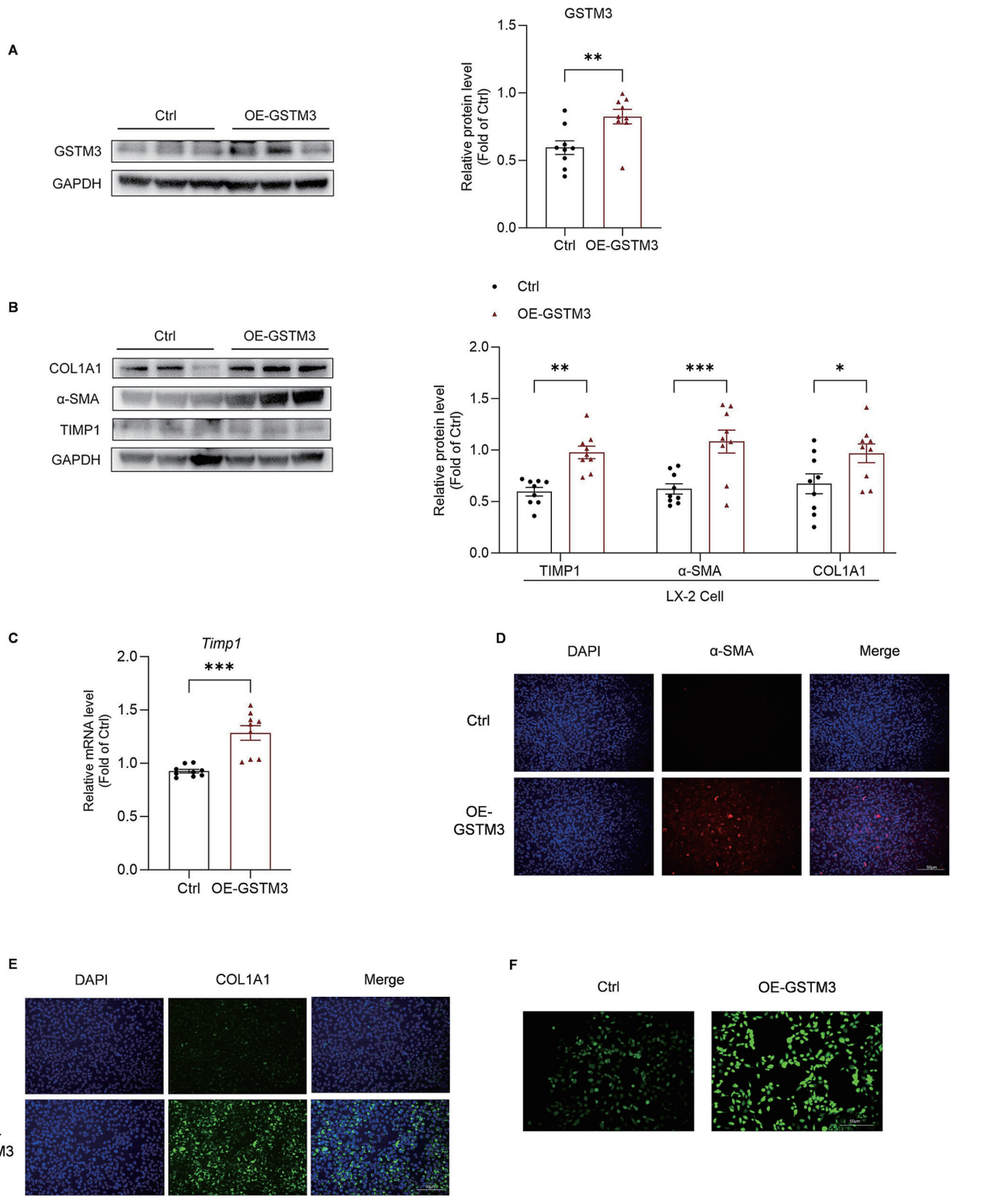

Fig. 6. Effects of GSTM3 overexpression on HSC activation and ROS levels in LX-2 cells. LX-2 cells were transfected with the pcDNA3.1-GSTM3 plasmid for 24 h (n = 3). (A) Western blot analysis of GSTM3 levels. (B) Western blot analysis of TIMP1, COL1A1, and α-SMA levels. (C) RT-qPCR analysis of *Timp1* mRNA expression levels. (D, E) Immunofluorescence staining for α-SMA and COL1A1. (F) ROS levels in LX-2 cells. Data are presented as mean ± SEM (**P* < 0.05; ***P* < 0.01; ****P* < 0.001). *P*-values were obtained using an unpaired *t*-test. GSTM3, glutathione S-transferase Mu 3; HSC, hepatic stellate cell; ROS, reactive oxygen species; TIMP1, tissue inhibitor of metalloproteinases 1; COL1A1, collagen type I alpha 1 chain; α-SMA, α-smooth muscle actin; RT-qPCR, reverse transcription quantitative polymerase chain reaction; SEM, standard error of the mean; GAPDH, glyceraldehyde-3-phosphate dehydrogenase.

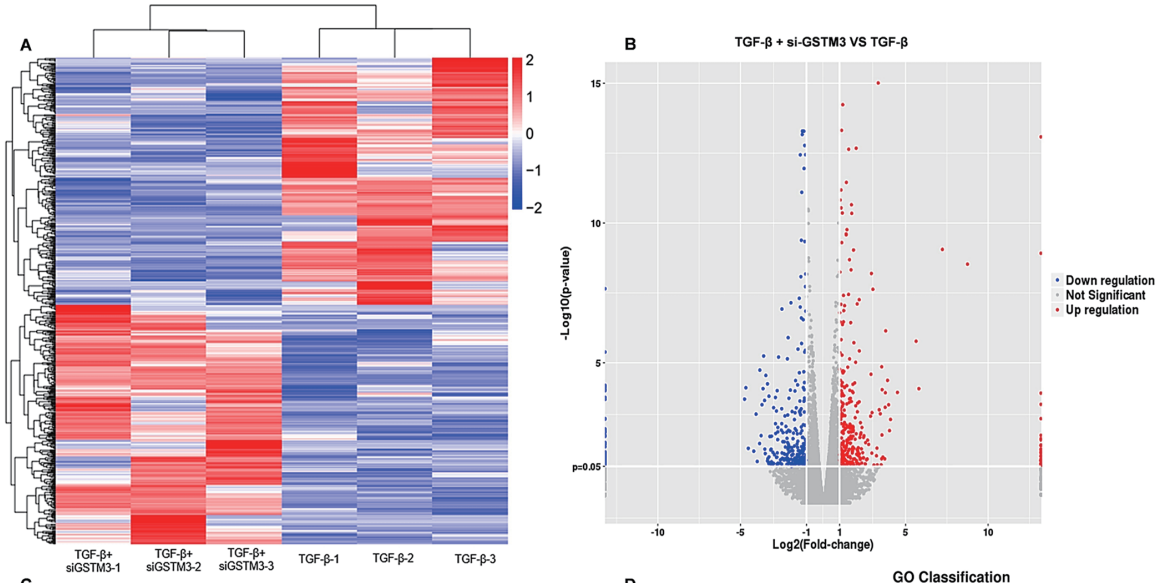

C

Pathway	P value
PPAR signaling pathway	0.027
Ras signaling pathway	0.041
Pathways in cancer	0.050
PI3K-Akt signaling pathway	0.064
Chemokine signaling pathway	0.075
Focal adhesion	0.087
Cytokine-cytokine receptor interaction	0.092
Proteoglycans in cancer	0.289
Calcium signaling pathway	0.446
Gap junction	1.000
Drug metabolism-cytochrome P450	1.000

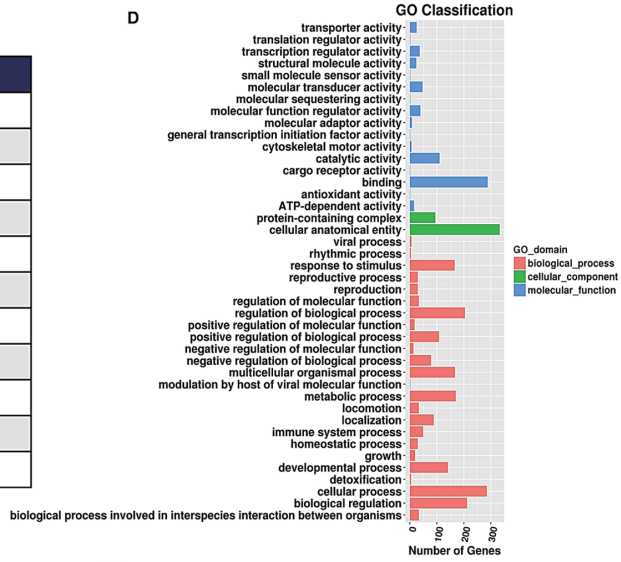

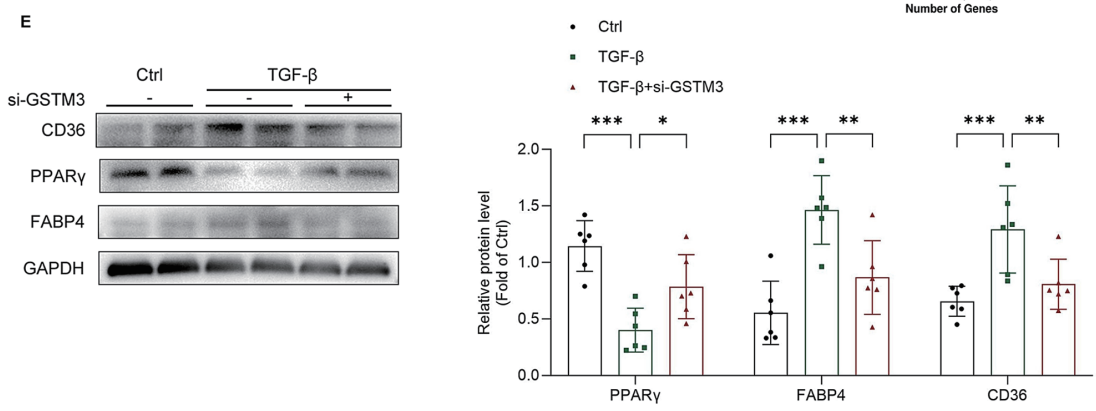

Fig. 7. Effects of GSTM3 knockdown on HSC activation via the PPARγ signaling pathway. LX-2 cells were transfected with si-GSTM3 for 12 h and then treated with or without TGF-β for 24 h (n = 3). (A, B) Heatmap and volcano plots of DEGs in LX-2 cells. (C) KEGG enrichment analysis of DEGs and a list of significantly enriched pathways based on *P*-values. (D) GO functional annotation analysis of DEGs. (E) Western blot analysis of PPARγ, FABP4, and CD36 levels. "+" and "−" indicate the presence and absence of si-GSTM3 transfection, respectively. Data are presented as mean ± SEM (*$P < 0.05$; **$P < 0.01$; ***$P < 0.001$). *P*-values were obtained using an unpaired *t*-test. GSTM3, glutathione S-transferase Mu 3; HSC, hepatic stellate cell; PPARγ, peroxisome proliferator-activated receptor γ; TGF-β, transforming growth factor-β; DEGs, differentially expressed genes; KEGG, Kyoto Encyclopedia of Genes and Genomes; GO, Gene Ontology; FABP4, fatty acid-binding protein 4; CD36, cluster of differentiation 36; SEM, standard error of the mean; GAPDH, glyceraldehyde-3-phosphate dehydrogenase.

β-treated LX-2 cells with or without GSTM3 knockdown and identified 647 DEGs. KEGG pathway enrichment analysis revealed that the DEGs were significantly enriched in pathways related to fibrosis, such as PPAR signaling, Ras signaling, and pathways in cancer, whereas GO annotation linked these genes to cellular processes and signal transduction, suggesting that GSTM3 modulates HSC activation through these pathways. Notably, systematic screening of the KEGG results and previous studies on fibrosis highlighted the PPARγ pathway as a key molecular mechanism.[50–54] PPARγ is a well-recognized negative regulator of HSC activation, and its activation inhibits HSC activation and attenuates fibrosis.[55–57] Our results confirmed that GSTM3 knockdown markedly upregulated PPARγ expression and attenuated the TGF-β-induced elevation of its downstream targets, CD36 and FABP4.[36,38] These data indicate that GSTM3 knockdown suppresses HSC activation and promotes fibrosis reversal, at least in part, through activation of the PPARγ signaling pathway.

Consistent with our findings in the mouse model of liver fibrosis, clinical sample analysis further supported the role of GSTM3 in liver fibrosis. In patients, GSTM3 expression in both liver tissue and serum increased gradually with fibrosis stage. Moreover, serum GSTM3 levels showed good diagnostic performance for fibrosis and cirrhosis and were positively correlated with the clinical fibrosis index FIB-4.[58] These clinical results not only verified the expression pattern of GSTM3 observed in our animal and proteomic analyses but also highlighted its potential as a novel diagnostic biomarker for liver fibrosis.

Nevertheless, this study has some limitations regarding the clinical specimens. Future longitudinal studies are warranted to collect serial liver tissue and serum samples from patients undergoing fibrosis reversal to further validate the dynamic changes in GSTM3 expression and strengthen its clinical value.

Conclusions

GSTM3 was identified as a novel regulator that is progressively downregulated during fibrosis reversal in mouse liver. GSTM3 knockdown promotes liver fibrosis reversal, which may be mediated by the inhibition of HSC activation via the PPARγ-FABP4-CD36 signaling pathway. Moreover, GSTM3 levels gradually increased with disease stage in the serum and liver tissue of patients with fibrosis; thus, GSTM3 may serve as a promising therapeutic target and diagnostic biomarker for liver fibrosis.

Supporting information

Supplementary material for this article is available at https://doi.org/10.14218/JCTH.2025.00658.

Acknowledgments

We thank Lei Sun and Kun Yang from the Department of Pathology, Beijing Ditan Hospital, for the pathological analysis of all liver tissues.

Funding

None to declare.

Conflict of interest

The authors have no conflict of interests related to this publication.

Author contributions

Conceived and mentored this study (YL, QW), designed and performed experiments, acquired and analyzed data, wrote the draft of the manuscript (CH, BY), and provided technical support and conceptual advice (YZ, HC, TB). All authors have approved the final version and publication of the manuscript.

Ethical statement

All protocols and animal studies were conducted in accordance with the Guide for the Care and Use of Laboratory Animals of the US National Institutes of Health (NIH Publication No. 85-23; National Academies Press, 2011) and were approved by the Animal Experiments and Experimental Animal Welfare Committee of Capital Medical University (No. AEEI-2024-486). All animals received human care. The human study conformed to the ethical guidelines of the 2024 Declaration of Helsinki, as reflected in a priori approval by the Ethics Committee of Beijing Ditan Hospital (No. KY2021-046-03 and No. KY2025-015-03), and the Informed Consent Form for Medical Data and Biological Sample Donation. All participants provided written informed consent. All biological samples and clinical data included in this retrospective analysis were fully anonymized before use. No additional interventions that might compromise patients' rights, interests or welfare were performed. Furthermore, no biological materials were obtained from prisoners or other vulnerable institutionalized populations.

Data sharing statement

Data supporting the findings of this study are available from the corresponding authors upon reasonable request.

References

[1] Kisseleva T, Brenner D. Molecular and cellular mechanisms of liver fibrosis and its regression. Nat Rev Gastroenterol Hepatol 2021;18(3):151–166. doi:10.1038/s41575-020-00372-7, PMID:33128017.
[2] Roehlen N, Crouchet E, Baumert TF. Liver Fibrosis: Mechanistic Concepts and Therapeutic Perspectives. Cells 2020;9(4):E875. doi:10.3390/cells9040875, PMID:32260126.
[3] Li M, Li C, Zuo D. Research advances on pathogenesis and related signal transduction mechanisms of hepatic fibrosis. Chin J Comp Med 2023;33(8):147–152. doi:10.3969/j.issn.1671-7856.2023.08.020.
[4] Devarbhavi H, Asrani SK, Arab JP, Nartey YA, Pose E, Kamath PS. Global burden of liver disease: 2023 update. J Hepatol 2023;79(2):516–537. doi:10.1016/j.jhep.2023.03.017, PMID:36990226.
[5] Burki T. WHO's 2024 global hepatitis report. Lancet Infect Dis 2024;24(6):e362–e363. doi:10.1016/S1473-3099(24)00307-4, PMID:38795729.
[6] Ganesan P, Kulik LM. Hepatocellular Carcinoma: New Developments. Clin Liver Dis 2023;27(1):85–102. doi:10.1016/j.cld.2022.08.004, PMID:36400469.
[7] Sun YM, Chen SY, You H. Regression of liver fibrosis: evidence and challenges. Chin Med J (Engl) 2020;133(14):1696–1702. doi:10.1097/CM9.0000000000000835, PMID:32568866.
[8] Li B, Yu D. Multiomic predictors for regression of cirrhosis: Clinical implications and future directions. ILIVER 2024;3(4):100116. doi:10.1016/j.iliver.2024.100116, PMID:40635855.
[9] Caligiuri A, Gentilini A, Pastore M, Gitto S, Marra F. Cellular and Molecular Mechanisms Underlying Liver Fibrosis Regression. Cells 2021;10(10):2759. doi:10.3390/cells10102759, PMID:34685739.
[10] Feng M, Ding J, Wang M, Zhang J, Zhu X, Guan W. Kupffer-derived matrix metalloproteinase-9 contributes to liver fibrosis resolution. Int J Biol Sci 2018;14(9):1033–1040. doi:10.7150/ijbs.25589, PMID:29989076.
[11] Zheng M, Li YY, Wang GF, Jin JY, Wang YH, Wang TM, *et al*. Protective effect of cultured bear bile powder against dimethylnitrosamine-induced hepatic fibrosis in rats. Biomed Pharmacother 2019;112:108701. doi:10.1016/j.biopha.2019.108701, PMID:30818137.
[12] Hayes JD, Pulford DJ. The glutathione S-transferase supergene family: regulation of GST and the contribution of the isoenzymes to cancer chemoprotection and drug resistance. Crit Rev Biochem Mol Biol 1995;30(6):445–600. doi:10.3109/10409239509083491, PMID:8770536.
[13] Brooks JD, Weinstein M, Lin X, Sun Y, Pin SS, Bova GS, *et al*. CG island methylation changes near the GSTP1 gene in prostatic intraepithelial neoplasia. Cancer Epidemiol Biomarkers Prev 1998;7(6):531–536.

PMID:9641498.
[14] Wang S, Yang J, You L, Dai M, Zhao Y. GSTM3 Function and Polymorphism in Cancer: Emerging but Promising. Cancer Manag Res 2020;12:10377–10388. doi:10.2147/CMAR.S272467, PMID:33116892.
[15] Hayes JD, Flanagan JU, Jowsey IR. Glutathione transferases. Annu Rev Pharmacol Toxicol 2005;45:51–88. doi:10.1146/annurev.pharmtox.45.120403.095857, PMID:15822171.
[16] Li D, Gao Q, Xu L, Pang S, Liu Z, Wang C, *et al*. Characterization of glutathione S-transferases in the detoxification of metolachlor in two maize cultivars of differing herbicide tolerance. Pestic Biochem Physiol 2017;143:265–271. doi:10.1016/j.pestbp.2016.12.003, PMID:29183603.
[17] Meding S, Balluff B, Elsner M, Schöne C, Rauser S, Nitsche U, *et al*. Tissue-based proteomics reveals FXYD3, S100A11 and GSTM3 as novel markers for regional lymph node metastasis in colon cancer. J Pathol 2012;228(4):459–470. doi:10.1002/path.4021, PMID:22430872.
[18] Chen Y, Feng Y, Lin Y, Zhou X, Wang L, Zhou Y, *et al*. GSTM3 enhances radiosensitivity of nasopharyngeal carcinoma by promoting radiation-induced ferroptosis through USP14/FASN axis and GPX4. Br J Cancer 2024;130(5):755–768. doi:10.1038/s41416-024-02574-1, PMID:38228715.
[19] Zhang Y, Sun N, Guo Y. Expression of GSTM5 in prostate cancer and its potential mechanisms in promoting cancer progression. J Xi'an Jiaotong Univ (Med Sci) 2023;44(1):100–106. doi:10.7652/jdyxb202301016.
[20] Guo J, Liang R, Chung A, Li Z, Li B, Chen E, *et al*. The origin of hepatocellular carcinoma depends on metabolic zonation. Science 2026;391(6784):eadv7129. doi:10.1126/science.adv7129, PMID:41196951.
[21] Zhang L, Zhou Q, Zhang J, Cao K, Fan C, Chen S, *et al*. Liver transcriptomic and proteomic analyses provide new insight into the pathogenesis of liver fibrosis in mice. Genomics 2023;115(6):110738. doi:10.1016/j.ygeno.2023.110738, PMID:37918454.
[22] Zhao S, Zhu Q, Lee WH, Funcke JB, Zhang Z, Wang MY, *et al*. The adiponectin-PPARγ axis in hepatic stellate cells regulates liver fibrosis. Cell Rep 2025;44(1):115165. doi:10.1016/j.celrep.2024.115165, PMID:39792554.
[23] Zhang Q, Xiang S, Liu Q, Gu T, Yao Y, Lu X. PPARγ Antagonizes Hypoxia-Induced Activation of Hepatic Stellate Cell through Cross Mediating PI3K/AKT and cGMP/PKG Signaling. PPAR Res 2018;2018:6970407. doi:10.1155/2018/6970407, PMID:29686697.
[24] Liu Y, Yin W. CD36 in liver diseases. Hepatol Commun 2025;9(1):e0623. doi:10.1097/HC9.0000000000000623, PMID:39774047.
[25] Li HL, Wu X, Xu A, Hoo RL. A-FABP in Metabolic Diseases and the Therapeutic Implications: An Update. Int J Mol Sci 2021;22(17):9386. doi:10.3390/ijms22179386, PMID:34502295.
[26] Sun G, Feng Z, Kuang Y, Fu Z, Wang Y, Zhao X, *et al*. Design, synthesis, and biological evaluation of piperazine derivatives as pan-PPARs agonists for the treatment of liver fibrosis. Eur J Med Chem 2024;269:116344. doi:10.1016/j.ejmech.2024.116344, PMID:38522113.
[27] Fang HL, Wu JB, Lin WL, Ho HY, Lin WC. Further studies on the hepatoprotective effects of Anoectochilus formosanus. Phytother Res 2008;22(3):291–296. doi:10.1002/ptr.2307, PMID:17886219.
[28] Wu YC, Wu Q, Yang Y, Yang F, Chen MZ. Changes of NF-κB and TGF-β1 in hepatic fibrosis and the effect of Hugan Pian (Hepatoprotective Tablet) on them. Chin J Antituberc 2007;29(4):317–320. doi:10.3969/j.issn.1000-6621.2007.04.008.
[29] Shao C, Lan W, Ding Y, Ye L, Huang J, Liang X, *et al*. JTCD attenuates HF by inhibiting activation of HSCs through PPARα-TFEB axis-mediated lipophagy. Phytomedicine 2025;139:156501. doi:10.1016/j.phymed.2025.156501, PMID:39978277.
[30] Chen J, Ge SJ, Feng HJ, Wu SZ, Ji R, Huang WR, *et al*. KRT17 Promotes the Activation of HSCs via EMT in Liver Fibrosis. J Clin Transl Hepatol 2022;10(2):207–218. doi:10.14218/JCTH.2021.00101, PMID:35528988.
[31] Zhang W, Cheng W, Fu J, Zeng R, Wang Z, Zhou J, *et al*. Integrated multi-omics unravels solanesol's multi-organ protection mechanisms against insulin resistance in type 2 diabetic mice. J Adv Res 2025. doi:10.1016/j.jare.2025.12.025, PMID:41456648.
[32] Wu BM, Liu JD, Li YH, Li J. Margatoxin mitigates CCl4-induced hepatic fibrosis in mice via macrophage polarization, cytokine secretion and STAT signaling. Int J Mol Med 2020;45(1):103–114. doi:10.3892/ijmm.2019.4395, PMID:31746414.
[33] Harms PW, Frankel TL, Moutafi M, Rao A, Rimm DL, Taube JM, *et al*. Multiplex Immunohistochemistry and Immunofluorescence: A Practical Update for Pathologists. Mod Pathol 2023;36(7):100197. doi:10.1016/j.modpat.2023.100197, PMID:37105494.
[34] Jin S, Zhang QY, Kang XM, Wang JX, Zhao WH. Daidzein induces MCF-7 breast cancer cell apoptosis via the mitochondrial pathway. Ann Oncol 2010;21(2):263–268. doi:10.1093/annonc/mdp499, PMID:19889614.
[35] Livak KJ, Schmittgen TD. Analysis of relative gene expression data using real-time quantitative PCR and the 2(-Delta Delta C(T)) Method. Methods 2001;25(4):402–408. doi:10.1006/meth.2001.1262, PMID:11846609.
[36] Kurien BT, Scofield RH. Western blotting. Methods 2006;38(4):283–293. doi:10.1016/j.ymeth.2005.11.007, PMID:16483794.
[37] Miao C, Ding Z, Wu J, An Q, Shu Y, Jiang H, *et al*. Identification and targeting oxidative phosphorylation/glycolysis to overcome anti-CSF-1R therapy resistance in glioblastoma. Cell Death Dis 2025;17(1):84. doi:10.1038/s41419-025-08288-3, PMID:41365876.
[38] Yu H, Guo J, Li B, Ma J, Abebe BK, Mei C, *et al*. Erucic acid promotes intramuscular fat deposition through the PPARγ-FABP4/CD36 pathway. Int J Biol Macromol 2025;298:140121. doi:10.1016/j.ijbiomac.2025.140121, PMID:39837435.
[39] Sun S, Duan X, Wu Q, Bu X, He Y, Ming X, *et al*. FABP4 Inhibitor Alleviates Lipopolysaccharide-Induced HUVEC Injury by Inactivating NF-κB and Activating PPARγ. Int Heart J 2024;65(6):1153–1160. doi:10.1536/ihj.24-272, PMID:39617505.
[40] Wang Y, Yi G, Tang C. Effects of high density lipoprotein 2 and 3 on expression of PPAR and CD36, and cellular lipid accumulation in THP-1 macrophages. Chin J Antituberc 2004;12(5):524–528. doi:10.3969/j.issn.1007-3949.2004.05.007.
[41] Dai Z, Liu X, Liang Y, Zhou G, Chen F, Xie W, *et al*. CD36-PPARγ-SPP1 axis mediates hepatocyte-macrophage coordination to drive MASLD-related liver fibrosis. JHEP Rep 2026;8(4):101745. doi:10.1016/j.jhepr.2026.101745, PMID:41810434.
[42] Wiering L, Subramanian P, Hammerich L. Hepatic Stellate Cells: Dictating Outcome in Nonalcoholic Fatty Liver Disease. Cell Mol Gastroenterol Hepatol 2023;15(6):1277–1292. doi:10.1016/j.jcmgh.2023.02.010, PMID:36828280.
[43] Lo RC, Kim H. Histopathological evaluation of liver fibrosis and cirrhosis regression. Clin Mol Hepatol 2017;23(4):302–307. doi:10.3350/cmh.2017.0078, PMID:29281870.
[44] Troeger JS, Mederacke I, Gwak GY, Dapito DH, Mu X, Hsu CC, *et al*. Deactivation of hepatic stellate cells during liver fibrosis resolution in mice. Gastroenterology 2012;143(4):1073–83.e22. doi:10.1053/j.gastro.2012.06.036, PMID:22750464.
[45] Krizhanovsky V, Yon M, Dickins RA, Hearn S, Simon J, Miething C, *et al*. Senescence of activated stellate cells limits liver fibrosis. Cell 2008;134(4):657–667. doi:10.1016/j.cell.2008.06.049, PMID:18724938.
[46] Kong D, Zhang F, Zhang Z, Lu Y, Zheng S. Clearance of activated stellate cells for hepatic fibrosis regression: molecular basis and translational potential. Biomed Pharmacother 2013;67(3):246–250. doi:10.1016/j.biopha.2012.10.002, PMID:23201010.
[47] Lee YS, Seki E. In Vivo and In Vitro Models to Study Liver Fibrosis: Mechanisms and Limitations. Cell Mol Gastroenterol Hepatol 2023;16(3):355–367. doi:10.1016/j.jcmgh.2023.05.010, PMID:37270060.
[48] Friedman SL. Liver fibrosis — from bench to bedside. J Hepatol 2003;38(Suppl 1):S38–S53. doi:10.1016/s0168-8278(02)00429-4, PMID:12591185.
[49] Parola M, Pinzani M. Liver fibrosis: Pathophysiology, pathogenetic targets and clinical issues. Mol Aspects Med 2019;65:37–55. doi:10.1016/j.mam.2018.09.002, PMID:30213667.
[50] Chen Z, Tian R, She Z, Cai J, Li H. Corrigendum to "Role of oxidative stress in the pathogenesis of nonalcoholic fatty liver disease" [Free Radic. Biol. Med. 152 (2020) 116-141]. Free Radic Biol Med 2021;162:174. doi:10.1016/j.freeradbiomed.2020.06.011, PMID:32571642.
[51] Gao H, Jin Z, Bandyopadhyay G, Wang G, Zhang D, Rocha KCE, *et al*. Aberrant iron distribution via hepatocyte-stellate cell axis drives liver lipogenesis and fibrosis. Cell Metab 2022;34(8):1201–1213.e5. doi:10.1016/j.cmet.2022.07.006, PMID:35921818.
[52] Zhao Q, Liu J, Deng H, Ma R, Liao JY, Liang H, *et al*. Targeting Mitochondria-Located circRNA SCAR Alleviates NASH via Reducing mROS Output. Cell 2020;183(1):76–93.e22. doi:10.1016/j.cell.2020.08.009, PMID:32931733.
[53] Luo P, Liu D, Zhang Q, Yang F, Wong YK, Xia F, *et al*. Celastrol induces ferroptosis in activated HSCs to ameliorate hepatic fibrosis via targeting peroxiredoxins and HO-1. Acta Pharm Sin B 2022;12(5):2300–2314. doi:10.1016/j.apsb.2021.12.007, PMID:35646542.
[54] Geng Q, Xu J, Cao X, Wang Z, Jiao Y, Diao W, *et al*. PPARG-mediated autophagy activation alleviates inflammation in rheumatoid arthritis. J Autoimmun 2024;146:103214. doi:10.1016/j.jaut.2024.103214, PMID:38648706.
[55] Chen Y, Xu YN, Ye CY, Feng WB, Zhou QT, Yang DH, *et al*. GLP-1 mimetics as a potential therapy for nonalcoholic steatohepatitis. Acta Pharmacol Sin 2022;43(5):1156–1166. doi:10.1038/s41401-021-00836-9, PMID:34934197.
[56] Kallwitz ER, McLachlan A, Cotler SJ. Role of peroxisome proliferators-activated receptors in the pathogenesis and treatment of nonalcoholic fatty liver disease. World J Gastroenterol 2008;14(1):22–28. doi:10.3748/wjg.14.22, PMID:18176957.
[57] Yu J, Zhang S, Chu ES, Go MY, Lau RH, Zhao J, *et al*. Peroxisome proliferator-activated receptors gamma reverses hepatic nutritional fibrosis in mice and suppresses activation of hepatic stellate cells in vitro. Int J Biochem Cell Biol 2010;42(6):948–957. doi:10.1016/j.biocel.2010.02.006, PMID:20156580.
[58] Sterling RK, Patel K, Duarte-Rojo A, Asrani SK, Alsawas M, Dranoff JA, *et al*. AASLD Practice Guideline on blood-based noninvasive liver disease assessment of hepatic fibrosis and steatosis. Hepatology 2025;81(1):321–357. doi:10.1097/HEP.0000000000000845, PMID:38489523.